ACS POLYMERS Au
AN OPEN ACCESS JOURNAL OF THE AMERICAN CHEMICAL SOCIETY

pubs.acs.org/polymerau
Article

Stimuli-Responsive Control over Self-Assembled Nanostructures in Sequence-Specific Functional Block Copolymers

Published as part of ACS Polymers Au virtual special issue "Polymer Science and Engineering in India".

Chirag Miglani, Jahanvi Ralhan, Maqsuma Banoo, Debasish Nath, Soma Sil, Santanu K. Pal, Ujjal K. Gautam, and Asish Pal*

Cite This: *ACS Polym. Au* 2024, 4, 255−265
Read Online

ACCESS | Metrics & More | Article Recommendations | Supporting Information

ABSTRACT: The precise sequence of a protein's primary structure is essential in determining its folding pathways. To emulate the complexity of these biomolecules, functional block copolymers consisting of segmented triblocks with distinct functionalities positioned in a sequence-specific manner are designed to control the polymer chain compaction. Triblock polymers **P-*b*-C-*b*-F** and **P-*b*-F-*b*-C** and random diblock copolymer **P-*b*-C-*r*-F** consist of a hydrophilic poly(ethylene oxide) (PEO) block and a hydrophobic block with coumarin (**C**) and ferrocene (**F**) moieties that are grafted in a sequence-specific or random manner onto the hydrophilic block. External stimuli such as UV_B light, redox, and chemical cues influence the functional hydrophobic block to alter the packing parameters that are monitored with spectroscopic and scattering techniques. Interestingly, the positioning of the stimuli-responsive moiety within the hydrophobic block of **P-*b*-C-*b*-F**, **P-*b*-F-*b*-C**, and **P-*b*-C-*r*-F** affects the extent of the hydrophobic−hydrophilic balance in block copolymers that renders orthogonal control in stimuli-responsive transformation of self-assembled vesicles to micelles.

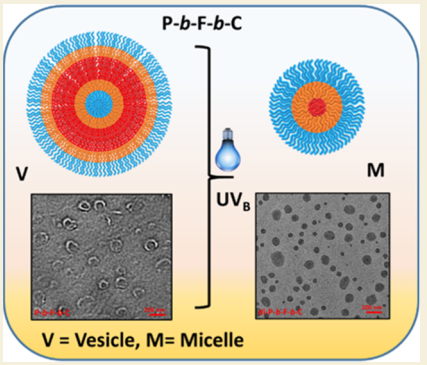

KEYWORDS: *block copolymer, self-assembly, sequence-specific, structural transformation, stimuli response*

INTRODUCTION

Proteins are structurally complex and functionally sophisticated among all molecules in a natural system and composed of hundreds of amino acids linked together in a long chain, giving rise to variable yet specific functions.[1−4] The sequence of amino acids dictate the primary structures, while a collection of noncovalent interactions controls the secondary structure to eventually organize the hierarchical tertiary structure to provide specific functions of the proteins. Such structure-functional precision exhibited by biopolymers is perhaps the challenging frontier in the design of synthetic polymers to mimic the complexity of the biomolecules. In that regard, efficient strategies such as controlled polymerization have emerged over the past few decades in a bid to precisely control the sequence of repeating units in block copolymers.[5−7] Thus, block copolymers with tunable compatibility among the blocks enable direct control over segregation ability that provide a driving force for self-assembly toward creating polymeric nanostructures.[8,9] This involves the variation of the monomer compositions throughout the chain length, introducing tapers at the block junction, or strategically placing comonomer-rich domains along the chain length to result in the formation of the desired morphology of nanostructures.[10−18] Segalman *et al.* designed polystyrene-*b*-polypeptoid diblock copolymers that differ in the sequence of comonomers in the polypeptoid block to tune the chain conformation, indicating the possibility of using sequence design to target a desired set of properties and morphologies in block copolymers.[19] In another example, Sosaki *et al.* synthesized triblock copolymers consisting of poly(oxyethylene) (PEO), poly(*d*-lactide) (PDLA), and poly(*l*-lactide) (PLLA) and demonstrated that the morphology of the micelles could be tuned by changing the core structures even at a constant hydrophilic/hydrophobic balance of the block chains.[20] Therefore, optimizing the sequence of monomers in the block copolymer chain can not only alter the dynamics of the chains, chain conformations, and morphologies but also enable the design of materials with predictable properties.[21−24] Consequently, the identification of an optimum balance between the hydrophobic and hydrophilic segments within the polymers is determined by packing parameters, ultimately leading to the formation of specific self-assembled nanostructures.[25−27] Notably, stimuli-responsive chain collapse could induce a change in the packing parameter,

Received: February 8, 2024
Revised: March 28, 2024
Accepted: March 28, 2024
Published: April 5, 2024

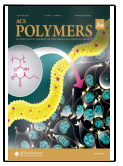

Scheme 1. Molecular Structure of the Block Copolymers Designed by RAFT Chain Extension Polymerization[a]

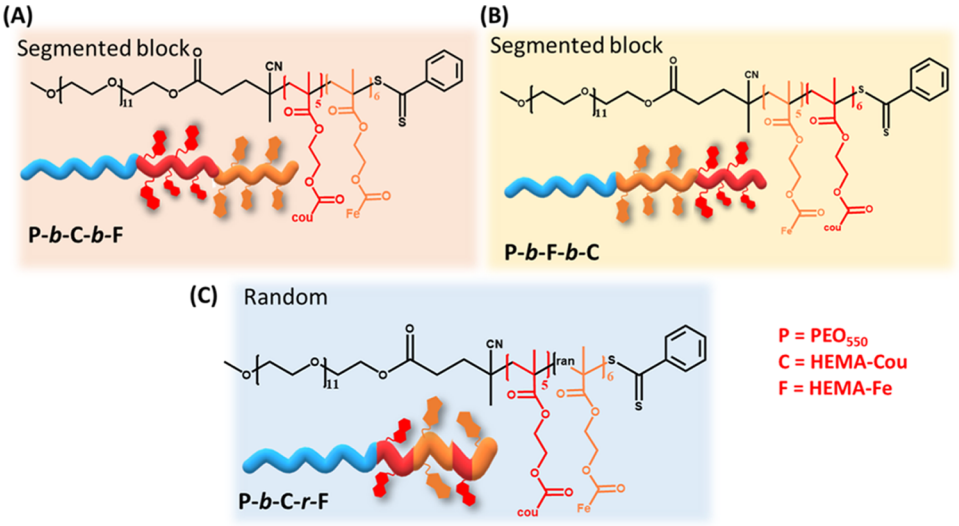

[a](A, B) Segmented triblock copolymers **P-*b*-C-*b*-F** and **P-*b*-F-*b*-C** and (C) random diblock copolymer **P-*b*-C-*r*-F.**

potentially resulting in a transformation of the self-assembled nanostructures.[28,29] Armes *et al.* demonstrated such stimuli-responsive chain collapse in the poly(*N*-(2-acryloyloxyethyl)-pyrrolidone)−poly(4-hydroxybutyl acrylate) ($PNAEP_{85}$−$PHBA_x$) diblock copolymer by increasing the pH of the dispersion above the pK_a of terminal carboxylic acid, leading to the chain-induced vesicle-to-sphere transition.[30] In another report, Harrison *et al.* reported reversible morphological transformations from spheres to worms and vesicles dictated by the pH of the surrounding medium in a pH-responsive copolymer composed of acrylic acid and butyl acrylate.[31,32] In that regard, our group demonstrated an interesting stimuli-responsive chain collapse strategy to alter polymeric nanostructures for application in photoresponsive self-healable coating and drug delivery applications.[33−35] Further, we have also exploited such stimuli-responsive polymer chain folding to design interesting peptide−polymer conjugate networks with exciting nonlinear mechanical properties and piezoelectric behavior.[36−39] Recently, we have demonstrated that an amphiphilic diblock polymer with stimuli-responsive moieties in the hydrophobic domain can exhibit chain collapse behavior in response to external stimuli, leading to reversible transformation of vesicles to micelles by fine-tuning the packing parameter.[40] Thus, the coassembled vesicles, influenced by orthogonal stimuli, formed self-sorted compartments, offering potential applications in mimicking interactions of artificial cell models with the extracellular matrix. In that regard, we explored chirality-driven compartmentalization in dynamic supramolecular polymers and covalent polymers, moving a step closer to imitating orthogonality in biological systems.[41−43] However, emulating the complexity of cellular systems demands the design of polymers with orthogonal stimuli-responsive moieties to achieve compartmentalization akin to biological systems. Thus, the synthesis of triblock copolymer systems further enhances the control, facilitating the development of compartmentalized structures that closely resemble the organization seen in biological systems. This approach enables us to replicate and study biological processes with a higher degree of precision and fidelity.

Herein, we synthesize segmented block copolymers with sequence-specific combinations of distinct functionalities positioned in different blocks (Scheme 1). Triblock polymers, namely, **P-*b*-C-*b*-F** and **P-*b*-F-*b*-C**, and a diblock, **P-*b*-C-*r*-F**, consist of a hydrophilic PEO block and hydrophobic blocks containing coumarin (**C**) and ferrocene (**F**) moieties. These moieties are grafted onto the PEO block in a sequence-specific or random manner. Further, the positioning of the stimuli-responsive moiety within the hydrophobic block plays a significant role in dictating the stimuli response to eventually alter the hydrophobic−hydrophilic balance. This imparts orthogonal control in controlling the packing parameter value in the block copolymers toward stimuli-responsive transformation of self-assembled vesicles into micelles for **P-*b*-C-*b*-F**, **P-*b*-F-*b*-C**, and **P-*b*-C-*r*-F**.

EXPERIMENTAL SECTION

Nuclear Magnetic Resonance (NMR)

NMR spectra were acquired on a 400 MHz Bruker. The chemical shifts were reported in parts per million and appeared downfield to tetramethylsilane (TMS) using the resonance of the deuterated solvent as an internal standard. Splitting patterns are designated as singlet (s), doublet (d), triplet (t), and multiplet (m).

Size Exclusion Chromatography (SEC)

Size exclusion chromatography (SEC) measurements were performed on the Malvern Omnisec instrument having an RI detector and a viscometer detector using a Shodex KD-806 M column and dimethylformamide (DMF) as an eluent (0.01 M LiBr additive) with a flow rate of 0.7 mL/min at a temperature of 35 °C. The results were analyzed using Omnisec software with PMMA as the conventional calibration standard for M_n, M_w, and PDI. The samples were prepared by filtering the solutions through a 0.2 μm nylon filter into a 2 mL glass vial.

Synthesis

All of the block copolymers were prepared following the RAFT approach (Scheme 2). Detailed synthetic procedures for the macro-RAFT agents and diblock polymers **P-*b*-C** and **P-*b*-F** characterization can be found in the electronic Supporting Information (Figures S1−S5).

P-*b*-C-*b*-F. For the synthesis of triblock polymer **P-*b*-C-*b*-F** using RAFT polymerization, monomers F-HEMA (35 mg, 0.101 mmol) and **P-*b*-C** (50 mg, 0.020 mmol) and initiator AIBN (3 mg, 0.02 mmol) were added to 1.5 mL of dioxane. The mixture was degassed

https://doi.org/10.1021/acspolymersau.4c00009
ACS Polym. Au 2024, 4, 255−265

Scheme 2. Synthesis of Segmented Block Polymers: (A) Triblock P-*b*-C-*b*-F, (B) Triblock P-*b*-F-*b*-C, and (C) Diblock P-*b*-C-*r*-F as Designed by RAFT Chain Extension Polymerization

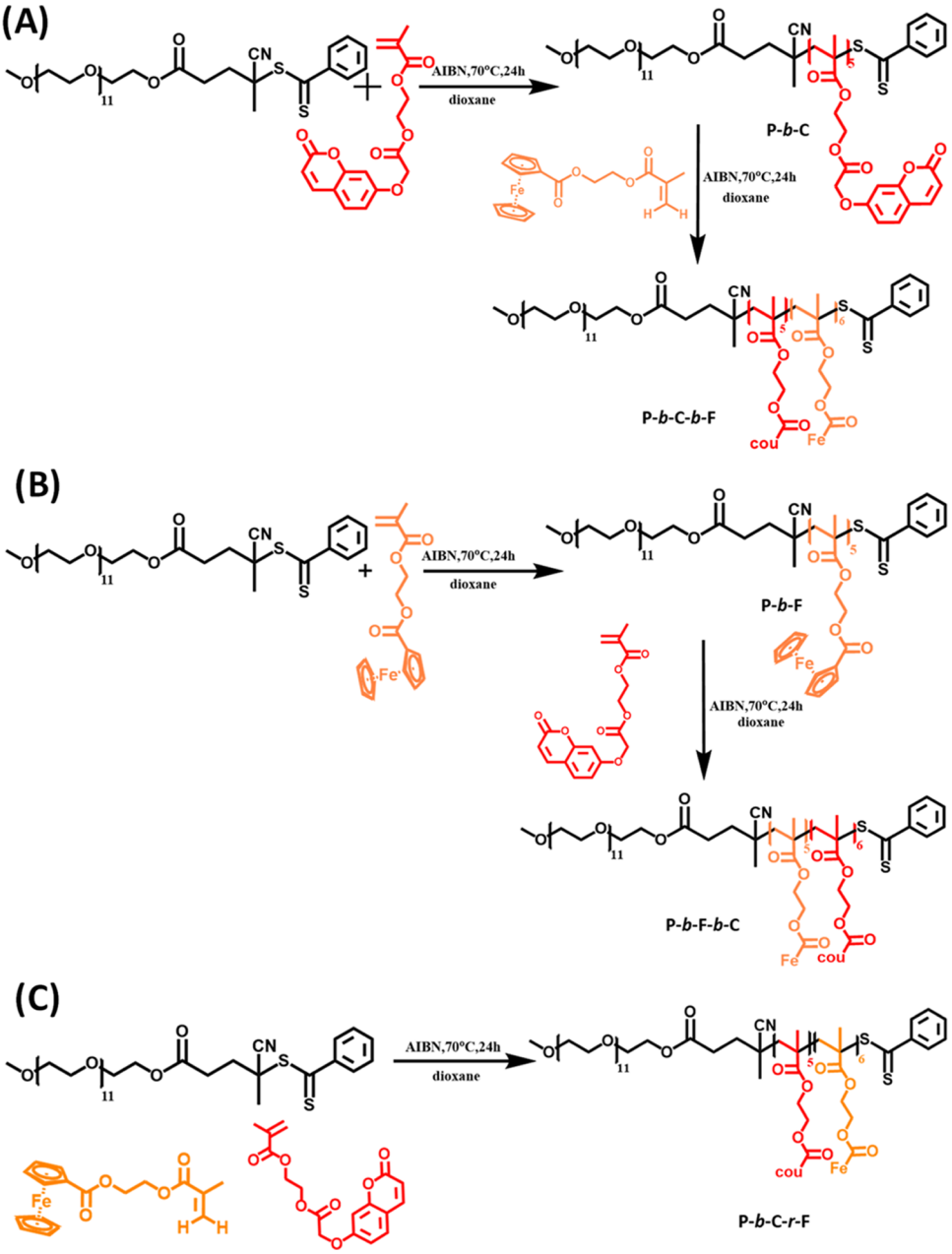

by N_2 bubbling and was further stirred at 70 °C under a N_2 environment for 24 h. After the reaction, the solution was precipitated in cold dry ether followed by centrifugation to get a white precipitate that was dried in vacuo to get the desired product.

^{1}H NMR (400 MHz, $CDCl_3$, 298 K) δ = 7.64 (m, 4H), 7.43 (m, 8H), 6.82 (m, 9H), 6.31(m, 3H), 4.81 (s, 7H), 4.72−4.3 (s, 48H), 4.3−4.0 (s, 67H), 3.71−3.5 (m, 51H), 1.21−0.88 (m, 51H).

SEC (DMF, PMMA standards): M_n = 4950 Da, M_w = 6170 Da, $Đ$ = 1.2.

P-*b*-F-*b*-C. Monomers C-HEMA (34 mg, 0.10 mmol) and **P-*b*-F** (50 mg, 0.020 mmol) and initiator AIBN (3 mg, 0.02 mmol) were added to 1.5 mL of dioxane. The mixture was degassed by N_2 bubbling and was further stirred at 70 °C under a N_2 environment for 24 h. After the reaction, the solution was precipitated in cold dry ether followed by centrifugation to get a white precipitate that was dried in vacuo to get the desired product

^{1}H NMR (400 MHz, $CDCl_3$, 298 K) δ = 7.61 (m, 7H), 7.40 (m, 7H), 6.86 (m, 14H), 6.24 (m, 6H), 4.81 (m, 16H), 4.2−4.10 (m, 36H), 3.8−3.5 (m, 51H), 1.4−1.03 (m, 57H).

SEC (DMF, PMMA standards): M_n = 4790 Da, M_w = 7640 Da, $Đ$ = 1.5.

P-*b*-C-*r*-F. Monomers C-HEMA (47 mg, 0.14 mmol), F-HEMA (49 mg, 0.14 mmol), and $mPEO_{11}$-CTP (23 mg, 0.028 mmol) and initiator AIBN (4 mg, 0.030 mmol) were added to 1.5 mL of dioxane. The mixture was degassed by N_2 bubbling and was further stirred at 70 °C under a N_2 environment for 24 h. After the reaction, the solution was precipitated in cold dry ether, followed by centrifugation to get a white precipitate that was dried in vacuo to get the desired product.

^{1}H NMR (400 MHz, $CDCl_3$, 298 K) δ = 7.64 (m, 4H), 7.43 (m, 8H), 6.82 (m, 9H), 6.31(m, 3H), 4.81 (m, 7H), 4.72−4.00 (m, 114H), 3.71−3.5 (m, 51H), 1.21−0.88 (m, 51H).

SEC (DMF, PMMA standards): M_n = 6150 Da, M_w = 7270 Da, $Đ$ = 1.2.

https://doi.org/10.1021/acspolymersau.4c00009
ACS Polym. Au 2024, 4, 255−265

Dynamic Light Scattering

Dynamic light scattering measurements were done on a Malvern Zetasizer Nano ZS ZEN3600 equipped with a helium−neon laser (wavelength, λ = 633 nm with a backscattering angle of 173°). Samples were prepared by filtering solutions through a 0.2 μm nylon filter into a glass cuvette.

Photodimerization Study

Ultraviolet (UV) cross-linking/de-cross-linking was performed using a UV chamber equipped with a 1 W × 8 W UV_B lamp (λ_{max} = 320 nm, intensity at 15 cm = 790 $\mu W/cm^2$) and a 1*8 W UV_C lamp (λ_{max} = 254 nm, intensity at 15 cm = 820 $\mu W/cm^2$), and the sample in the liquid state was kept at a distance of 15 cm for irradiation. The luminous intensity of irradiation at time t was determined in J/cm^2 by the formula $[(\mu W/cm^2)/10^6] \times t(s)$. UV−visible (UV−vis) spectra were recorded using an Agilent Cary 60 spectrophotometer in a wavelength range of 800−200 nm.

Electrochemical Measurement

Cyclic voltammetry (CV) studies were performed on a Metrohm MULTI AUTOLAB M204 potentiostat/galvanostat using a standard three-electrode system. The cyclic voltammetry (CV) experiment was conducted at room temperature using a three-electrode system consisting of a working electrode (**P-*b*-C-*b*-F**, **P-*b*-F-*b*-C**, and **P-*b*-C-*r*-F** on a Nafion-coated glassy carbon electrode), a platinum electrode as the auxiliary electrode, and a Ag/AgCl electrode as the reference electrode. The CV data analysis was performed using Nova 1.11 software. The CV studies were carried out using a 10 mM phosphate buffer as the primary analyte solution and scanned over a potential range from −0.4 to +0.8 V. Polymer samples were prepared in ethanol and drop-cast onto the Nafion-coated glassy carbon electrode, followed by drying for 30 min.

Microscopic Studies

The polymer samples were drop-cast on a 300 mesh carbon-coated copper grid with uranyl acetate as a staining agent, and TEM images were recorded using a JEOL JEM-F200 with a Tungsten filament at an accelerating voltage of 200 kV.

Langmuir−Blodgett

Polymer monolayers were prepared by using a KSV Nima Langmuir−Blodgett trough that was placed horizontally within a Plexiglas box to avoid surface contamination. The surface pressure measurements were performed by using a filter paper Wilhelmy plate. The trough was filled with Milli-Q water. Polymers **P-*b*-C-*b*-F**, **P-*b*-F-*b*-C**, and **P-*b*-C-*r*-F** were dissolved in chloroform at a concentration of 1 mg/mL and added dropwise on the surface of Milli-Q water. Chloroform was allowed to evaporate for 10 min after the addition of a known volume of polymer solution. The barriers were then allowed to compress symmetrically at a compression rate of 10 mm/min. The surface pressure versus area per molecule was obtained by using KSV Nima software.

RESULTS AND DISCUSSION

Design and Characterization of Block Copolymers

We designed a macroinitiator with a poly(ethylene oxide) group as a hydrophilic block via RAFT polymerization using 4-cyano-4-[(phenylcarbonothioyl)thio]pentanoic acid as the raft reagent. To this hydrophilic macroinitiator, a hydrophobic block of either coumarin- or ferrocene-tethered 2-hydroxymethyl methacrylate was grafted in a sequence-specific or random manner via chain extension to result in a segmented block copolymer system (Scheme 2). The polymers were characterized using ^{1}H NMR with the characteristic peak of coumarin in the region of δ = 6−7.5 ppm and the ferrocene peak in the region of δ = 4.2−4.5 ppm. The PEO peak was located in the region of δ = 3.2−3.7 ppm, indicating the formation of a triblock polymer system. The percentage grafting of the coumarin and ferrocene group was calculated by comparing the collective integral of the protons composed of coumarin and ferrocene groups with that of the collective integral proton of the PEO chain as calculated from ^{1}H NMR (*cf.* ESI). Table 1 summarizes the characteristics of the polymers, including the percentage grafting as calculated from ^{1}H NMR, molecular weight (M_n, M_w), and $Đ$ values based on SEC analysis, for each polymer (Figures S6−S10). For **P-*b*-C-*b*-F**, the coumarin- and ferrocene-grafted blocks' degree of polymerization (DP) values were found to be n = 5 and m = 6, respectively. Similarly, in **P-*b*-F-*b*-C**, the DP values of coumarin- and ferrocene-grafted blocks were found to be n = 6 and m = 5, respectively. In the case of random triblock polymer **P-*b*-C-*r*-F**, the coumarin- and ferrocene-grafted blocks' DP values were found to be n = 5 and m = 6, respectively. SEC analysis of the polymers exhibited excellent control over molecular weight and the polydispersity index ($Đ$) in the range of 1.2−1.5.

Table 1. Characterization Details of the Triblock Polymers

	feed ratios		DP[a]				
polymer	Cou	Fc	Cou	Fc	M_n[b] (Da)	M_w[b] (DA)	$Đ$[b]
P-*b*-C-*b*-F	5	5	5 ± 2	6 ± 2	4952	6171	1.2
P-*b*-F-*b*-C	5	5	5 ± 2	6 ± 2	4792	7644	1.5
P-*b*-C-*r*-F	5	5	5 ± 2	6 ± 2	6150	7267	1.2

[a]Determined by ^{1}H NMR. [b]Determined by the SEC analyses in DMF (0.01 M LiBr) using pMMA as the standard (polymer concentration for SEC = 6 mg/mL in DMF (0.01 M LiBr)).

Photodimerization-Mediated Chain Collapse of the Polymers

The coumarin moiety exhibits the ability to undergo photodimerization upon irradiation with UV_B light. In this regard, segmented triblock polymers **P-*b*-C-*b*-F** and **P-*b*-F-*b*-C** and random diblock polymer **P-*b*-C-*r*-F** were dissolved in a 0.5% DMF−water mixture to a final concentration of 0.01 mM. The coumarin motif in the polymers showed characteristic absorption in the wavelength range of 290−330 nm that upon UV_B irradiation rendered a gradual hypochromic shift (Figure 1A−C). This could be attributed to the formation of the $[2\pi + 2\pi]$ cyclobutane adduct between coumarin moieties for polymers **P-*b*-C-*b*-F**, **P-*b*-F-*b*-C**, and **P-*b*-C-*r*-F**. Interestingly, the hypochromic shift was found to be much higher in the case of **P-*b*-F-*b*-C** and **P-*b*-C-*r*-F** as compared to **P-*b*-C-*b*-F** where coumarin was present in the inner block. Since coumarin moieties were grafted in a sequence-specific or random manner onto the hydrophilic PEO block, the coumarin present in the inner block of the triblock polymer responded differently from the coumarin present in the peripheral block or at random positions. Thus, the degree of photodimerization (%PD) calculated from UV−visible spectral analysis inferred that polymer **P-*b*-C-*b*-F** having coumarin in the inner block exhibited a low %PD of ∼17% (Figure 1D). In the case of **P-*b*-F-*b*-C**, the coumarin moieties exhibited a much higher %PD of ∼61%. However, the random distribution of coumarin in random copolymer **P-*b*-C-*r*-F** showed intermediate photodimerization efficacy (∼45%). This was in agreement with the fact that the position of coumarin within the hydrophobic block significantly influenced the photodimerization efficacy owing to the steric factors. This led us to conclude that the

https://doi.org/10.1021/acspolymersau.4c00009
ACS Polym. Au 2024, 4, 255−265

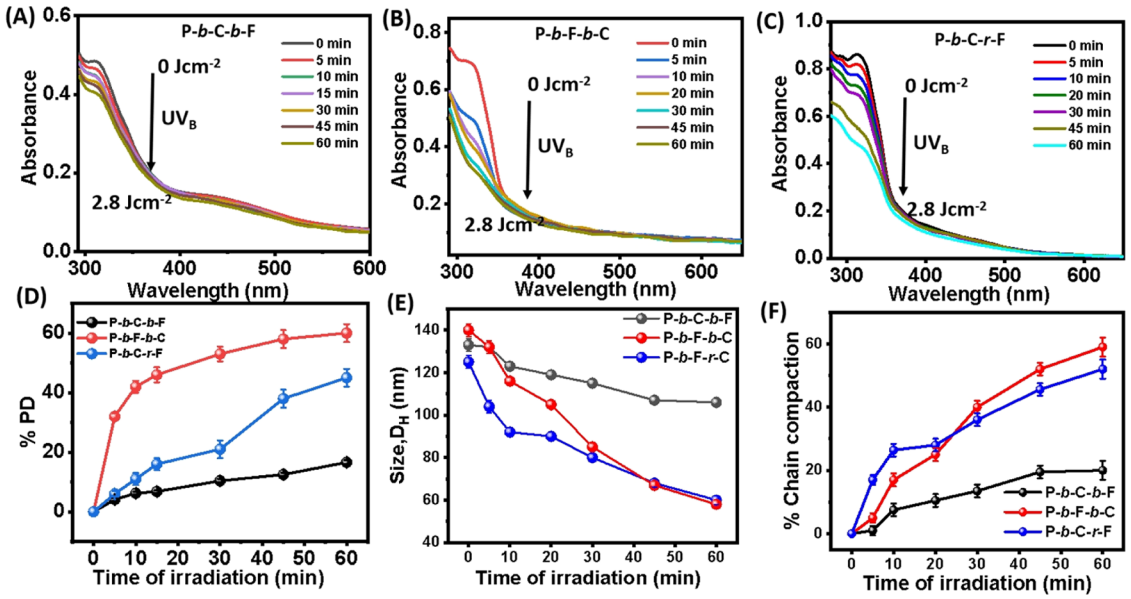

Figure 1. Monitoring photodimerization of the coumarin motifs in (A) **P-*b*-C-*b*-F**, (B) **P-*b*-F-*b*-C**, and (C) **P-*b*-C-*r*-F** using UV−vis spectra. (D) Degree of photoisomerization (%PD) of **P-*b*-C-*b*-F**, **P-*b*-F-*b*-C**, and **P-*b*-C-*r*-F** with increasing irradiation time. (E, F) DLS data showing a decrease in hydrodynamic diameter (D_H) and corresponding % chain compaction for polymers **P-*b*-C-*b*-F**, **P-*b*-F-*b*-C**, and **P-*b*-C-*r*-F** with increasing irradiation time UV_B lamp: 1 W × 8 W, [polymer] = 0.01 mM in 0.5% DMF−water.

position of coumarin is an important factor in determining photodimerization efficacy, thereby controlling the eventual chain collapse in the couramin-tethered polymers as previously reported by us.[33,34] Furthermore, the DLS experiment exhibited a reduction in hydrodynamic diameters upon UV_B irradiation due to the chain collapse in the hydrophobic blocks of polymers **P-*b*-C-*b*-F**, **P-*b*-F-*b*-C**, and **P-*b*-C-*r*-F**, as corroborated from intensity, volume, and number data (Figures 1E,F and S11). Moreover, % compaction was found to depend on the position of coumarin in triblock polymers owing to differential %PD efficacy. Thus, **P-*b*-C-*b*-F** exhibited the least chain collapse, i.e., 19%, while the other block copolymers where the position of coumarin was either peripheral (**P-*b*-F-*b*-C** 59%) or in a random fashion (**P-*b*-C-*r*-F** ∼ 51%) showed enhanced chain collapse (Figure 1F). Table 2 shows the chain compaction of the native polymers

Table 2. Characterization Details of the Polymers after UV_B Irradiation, Oxidation, and Host−Guest

		size, D_H (nm) @ stimuli[a]		
polymer	native size, D_H (nm)[a]	UV_B	$Fe(ClO_4)_3$	*bis*-β-CD
P-*b*-C-*b*-F	130 ± 5	105 ± 3	68 ± 5	68 ± 2
P-*b*-F-*b*-C	135 ± 5	57 ± 3	120 ± 5	70 ± 2
P-*b*-C-*r*-F	125 ± 5	60 ± 2	80 ± 5	55 ± 2

[a]Diameters were determined by the dynamic light scattering studies.

(D_H ∼ 130 nm) to a hydrodynamic diameter of ∼60−105 nm, depending upon the position of the coumarin moiety in the block copolymers.

Redox Response of the Polymers

Next, we explored polymers **P-*b*-C-*b*-F**, **P-*b*-F-*b*-C**, and **P-*b*-C-*r*-F** for their oxidation propensities by adding an oxidizing agent to understand the effect of the position of ferrocene in the block copolymer systems. Upon addition of 0.5 equiv of $Fe(ClO_4)_3$ as an oxidizing agent to the polymer solution of **P-*b*-C-*b*-F**, the yellow-colored solution of the polymer turned dark green, indicating the formation of a ferrocenium cation (Figure 2A−C). While **P-*b*-C-*r*-F** also showed the appearance of green color, **P-*b*-F-*b*-C** did not exhibit any significant color change. In that regard, the formation of the ferrocenium cation was monitored using UV−vis spectra, which showed the appearance of a new peak at 630 nm, a characteristic peak corresponding to the ferrocenium ion. Upon addition of 0.5 equiv of the reducing agent (ascorbic acid) to the above solution, the ferrocenium cation was reduced back to ferrocene with an obvious color change to yellow and the disappearance of the characteristic ferrocenium ion peak at 630 nm (Figure S12). However, the redox efficacy of the grafted ferrocene moieties was found to be position-dependent. When the ferrocene moieties were grafted at the periphery of the triblock polymer as in **P-*b*-C-*b*-F**, it exhibited a high oxidation propensity, i.e., 31%, as compared to the other triblock systems, i.e., **P-*b*-F-*b*-C** (5%) and **P-*b*-C-*r*-F** (10%; Figure 2D). The distance between the redox center, i.e., ferrocene, and the electrode surface holds relevance in defining the effect of a hindered environment on the oxidation ability of ferrocene.[44,45] In order to understand the effect of the position of ferrocene on its redox behavior in triblock polymer systems, we employed cyclic voltammetry, which highlighted reversible oxidation processes in the ferrocene-grafted polymers at approximately ∼0.4−0.6 V. Thus, **P-*b*-C-*b*-F** displayed higher electrochemical redox potential in comparison to **P-*b*-F-*b*-C** and **P-*b*-C-*r*-F**, which is in corroboration with spectroscopic results (Figure 2E).

The synthesized block copolymers had an optimal balance of hydrophobic and hydrophilic segments, thereby governing their self-assembly. Typically, the self-assembly of the polymer into a particular nanostructure is governed by the packing parameter value as provided in eq 1

$$P = \frac{v}{al} \tag{1}$$

https://doi.org/10.1021/acspolymersau.4c00009
ACS Polym. Au 2024, 4, 255−265

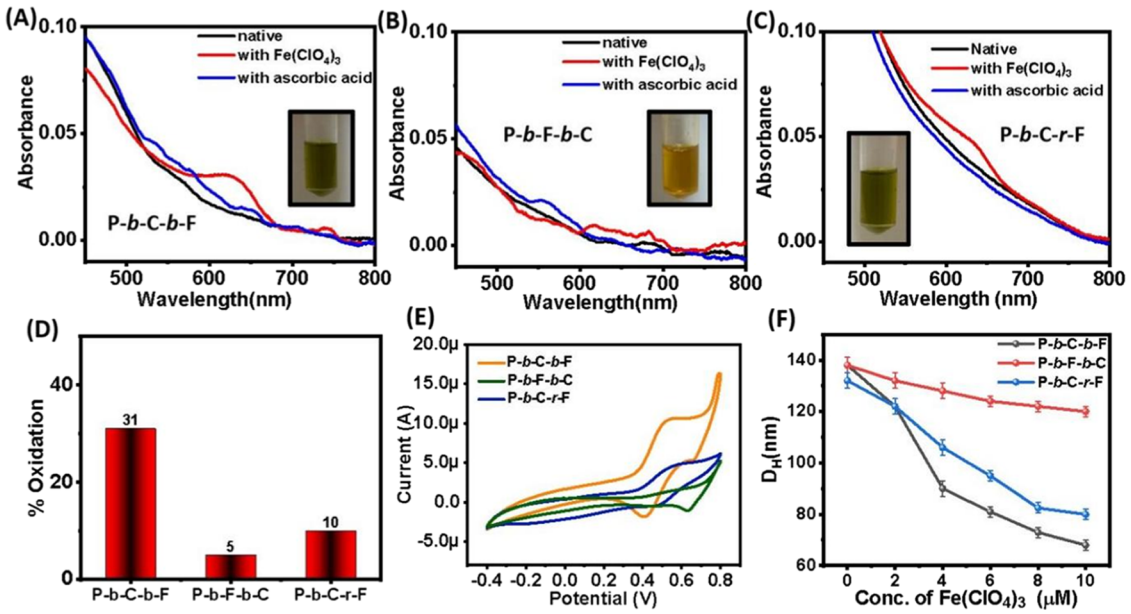

Figure 2. Monitoring redox-responsive behavior of ferrocene in (A) **P-*b*-C-*b*-F**, (B) **P-*b*-F-*b*-C**, and (C) **P-*b*-C-*r*-F** by UV−vis spectra. (D) Bar graph displaying %oxidation tendency in triblock polymers. (E) Cyclic voltammetric analysis showing redox responsiveness of polymers **P-*b*-C-*b*-F**, **P-*b*-F-*b*-C**, and **P-*b*-C-*r*-F**. (F) DLS data showing a decrease in hydrodynamic diameter (D_H) for polymers **P-*b*-C-*b*-F**, **P-*b*-F-*b*-C**, and **P-*b*-C-*r*-F** upon oxidation with $Fe(ClO_4)_3$ ([polymer] = 0.01 mM in 0.5% DMF−water; [$Fe(ClO_4)_3$] = 0.05 mM; [ascorbic acid] = 0.05 mM).

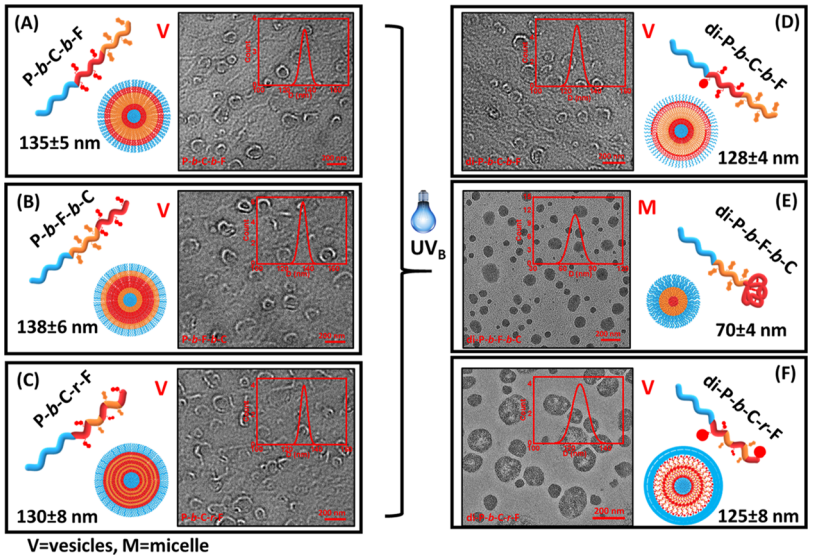

Figure 3. TEM images of native polymer vesicles with schematic representation for (A) **P-*b*-C-*b*-F**, (B) **P-*b*-F-*b*-C**, and (C) **P-*b*-C-*r*-F** to demonstrate self-assembly. TEM images of the polymer nanostructures after irradiation with UV_B light for 60 min show (D) no change in morphology in **P-*b*-C-*b*-F**, (E) formation of micelles in **P-*b*-F-*b*-C**, and (F) retention of vesicles with patches of chain compaction in **P-*b*-C-*r*-F**. Scale bar = 200 nm. ([polymer] = 0.001 mM in 0.5% DMF−water).

where v and l are the volume and length of the hydrophobic tail, respectively, and a is the optimal hydrophilic headgroup area.

However, in the presence of an oxidizing agent, the oxidation of ferrocene to the ferrocenium cation led to an increase in the hydrophilicity of the triblock polymers. As a consequence, it resulted in increased interactions with the aqueous media, which in turn demonstrated a reduction in the size of the nanostructures,[45,46] as evident from the DLS data (Figure 2F). This was further corroborated by SEC data that showed a shift in the retention volume of native **P-*b*-C-*b*-F** upon oxidation with redox stimuli (Figure S13). However, orthogonal light stimuli did not result in any shift in the SEC peak position owing to the low mobility of the inner coumarin block. The polymers showed a reduction in size mediated by oxidation; however, the reduction pattern was found to be different for all of the polymers. As the redox behavior was affected by the position of ferrocene grafting in the block copolymer system, the hydrophobic-to-hydrophilic transition via oxidation was found to be different for segmented triblock and random diblock polymers. The detailed size compaction data of all of the polymers with respect to redox stimuli are given in Table 2.

https://doi.org/10.1021/acspolymersau.4c00009
ACS Polym. Au 2024, 4, 255−265

Sequence-Specific Morphological Transformation of Polymers

In order to determine the morphology of the self-assembled polymers upon external stimuli, we utilized transmission electron microscopy (TEM). The amphiphilic block copolymers in the native state self-assembled into vesicles of sizes ranging between ∼130 and 140 nm with bilayer thicknesses of ∼13 and 15 nm (Figure 3A−C). Next, the amphiphilic balance of the polymeric systems was altered by stimuli-mediated chain collapse of the hydrophobic block. Thus, external stimuli such as UV_B, host−guest, and redox were expected to result in the transformation of the vesicle nanostructures. Upon irradiation of the native polymers with UV_B light, the photodimerization of coumarin moieties resulted in a decrease in the volume of the hydrophobic blocks of the polymer. A decrease in the volume of the hydrophobic compartment rendered a subsequent decrease in the packing parameter value, thus leading to the structural transformation of the vesicles (∼135 nm) to micelles of ∼70 nm diameter in the case of **P-*b*-F-*b*-C** (Figure 3E).[45] However, **P-*b*-C-*r*-F** exhibited chain compaction behavior in patches with the retention of vesicles of ∼125 nm, whereas no morphological transformation was observed in the case of **P-*b*-C-*b*-F** with coumarin as an inner block (Figure 3D,F). Table 3 summarizes the characteristics of the morphological transformation from vesicles to micelles in response to photo and redox stimuli based on TEM analysis. Such morphological analysis corroborated with the observations obtained from UV−vis and DLS data, highlighting the importance of the sequence specificity of the coumarin moiety in block copolymer systems.

Table 3. Characterization Details of the Polymers after UV Irradiation and Oxidation

		size, *d* (nm) @ stimuli[a]	
polymer	native size, *d*(nm)[a]; bilayer thickness (nm)	UV_B	$Fe(ClO_4)_3$
P-*b*-C-*b*-F	130 ± 5; 14	128 ± 3	75 ± 5
P-*b*-F-*b*-C	138 ± 5; 13	70 ± 3	120 ± 5
P-*b*-C-*r*-F	130 ± 5; 15	125 ± 2	100 ± 5

[a]Diameters were determined by the TEM.

Next, we investigated the effect of oxidation over polymeric self-assembly and consequent morphological transformation owing to alteration in the hydrophobicity of the polymer. The oxidizing agent $Fe(ClO_4)_3$ rendered ferrocene oxidation, leading to selective modulation in the hydrophobic polymer chain to transform self-assembled vesicles to micelles or aggregates for triblock polymers (Figure 4A−F).[47,48] Thus, **P-*b*-C-*b*-F** exhibited a transition from vesicles of sizes ranging between ∼130 and 140 nm (bilayer thicknesses ∼13−15 nm) to micelles (∼75 nm) due to oxidation of ferrocene to the ferrocenium cation that led to its increased interactions with the surrounding aqueous medium (Figure 4D). This resulted in an increase in the area of the hydrophilic headgroup, which in turn decreased the packing parameter, as evident from the formation of micelles in response to the redox cue. In contrast, polymer **P-*b*-F-*b*-C** displayed the least response to oxidation owing to the positioning of ferrocene in the inner block of the triblock polymer (Figure 4E).[48,49] Interestingly, for **P-*b*-C-*r*-F**, the random arrangement of ferrocene resulted in the disassembly of the vesicles and formation of swelled micellar aggregates upon oxidation (Figure 4F).[50] Such swelling was a consequence of enhanced interactions between the ferrocenium ion and its aqueous microenvironment, which led to the formation of comparatively large-sized micelles. Thus, for triblock polymers **P-*b*-C-*b*-F** and **P-*b*-F-*b*-C** and random diblock **P-*b*-C-*r*-F**, the selective chain compaction in the polymer segments provided orthogonally controlled transformation of the self-assembled vesicles into micelles in response to external stimuli such as light and redox cues.

Further, the triblock and random diblock polymeric systems containing coumarin and ferrocene grafts in their hydrophobic compartments demonstrated a high propensity to form host−guest inclusion complexes with bis-*β*-cyclodextrin (*bis*-*β*-CD) as the host. We studied the formation of host−guest complexes by UV−vis spectra that displayed an increase in absorbance in the wavelength range of 300−350 nm for all of the triblock

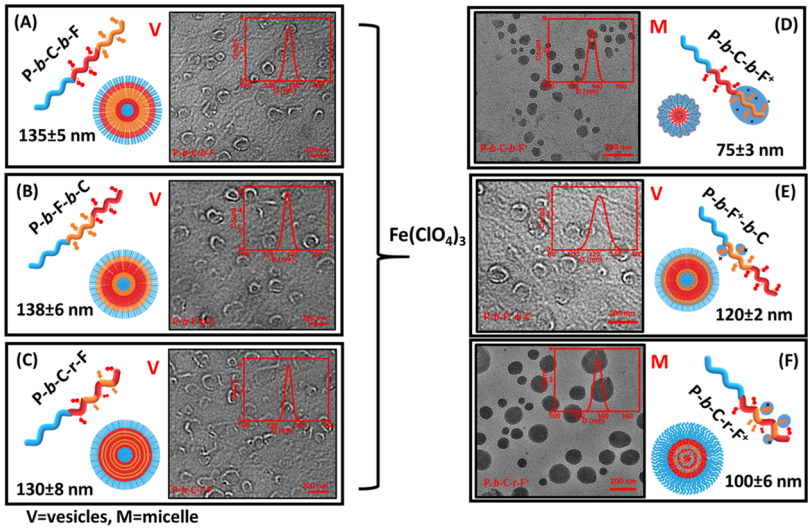

Figure 4. Schematic representation to demonstrate self-assembly and TEM images of native polymer vesicles for (A) **P-*b*-C-*b*-F**, (B) **P-*b*-F-*b*-C**, and (C) **P-*b*-C-*r*-F**. TEM images of the polymer nanostructures after oxidation with $Fe(ClO_4)_3$ show (D) formation of micelles of **P-*b*-C-*b*-F**, (E) no change in morphology of **P-*b*-F-*b*-C**, and (F) formation of swelled micelles of **P-*b*-C-*r*-F**. Scale bar = 200 nm, [polymer] = 0.001 mM in 0.5% DMF−water, $Fe(ClO_4)_3$ = 0.005 mM.

https://doi.org/10.1021/acspolymersau.4c00009
ACS Polym. Au 2024, 4, 255−265

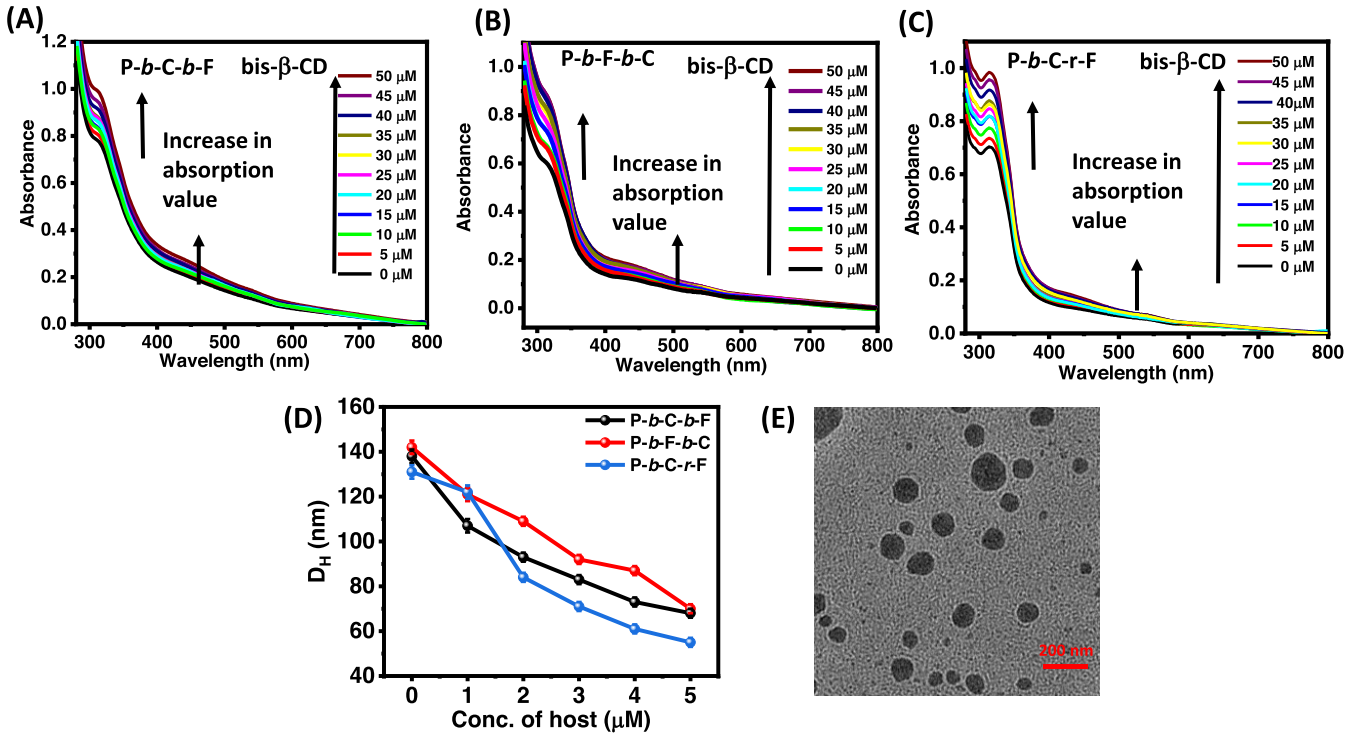

Figure 5. Monitoring the host−guest interaction with host bis-β-CD. (A−C) UV−vis spectra for **P-*b*-C-*b*-F**, **P-*b*-F-*b*-C**, and **P-*b*-C-*r*-F**. (D) Graph showing a decrease in hydrodynamic diameter (D_H) for polymers **P-*b*-C-*b*-F**, **P-*b*-F-*b*-C**, and **P-*b*-C-*r*-F** upon complexation with the host. (E) TEM image highlighting the morphological transformation from vesicles to micelles upon complexation. [polymer] = 0.01 mM in 0.5% DMF−water.

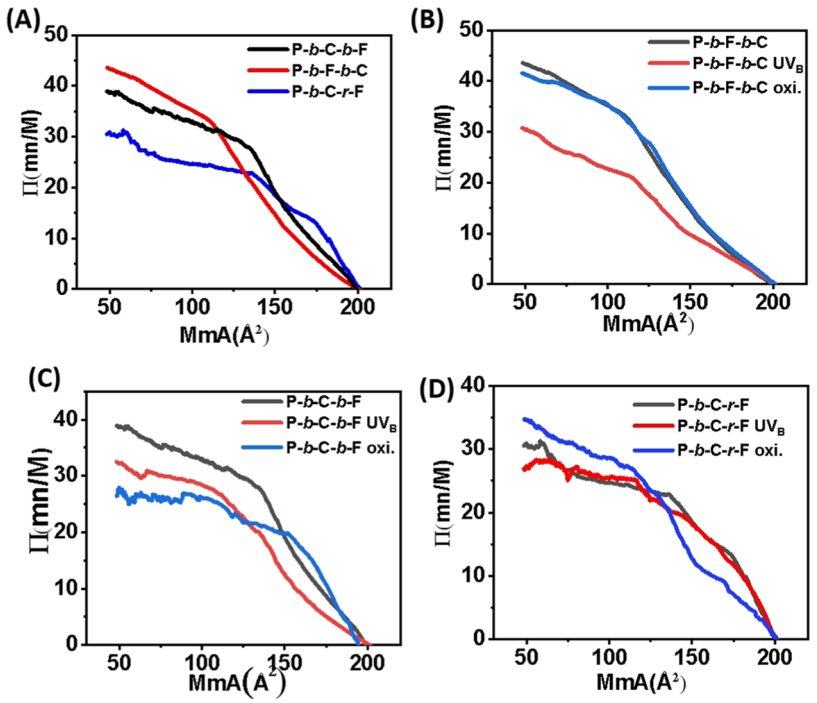

Figure 6. Comparative Langmuir isotherms of the native polymers (A) **P-*b*-C-*b*-F**, **P-*b*-F-*b*-C**, and **P-*b*-C-*r*-F**. Langmuir isotherm of polymers (B) **P-*b*-F-*b*-C**, (C) **P-*b*-C-*b*-F**, and (D) **P-*b*-C-*r*-F** upon application of UV_B light and redox stimuli in an orthogonal manner.

polymers upon adding the host (Figure 5A−C). The corresponding Job's plots suggested the formation of 1:1 inclusion complexes with respect to both coumarin and ferrocene in the case of **P-*b*-F-*b*-C** and **P-*b*-C-*b*-F** (Figure S14). Moreover, 2D-NOESY NMR spectra showed correlation peaks indicating through-space interactions between the coumarin and ferrocene moieties of polymers **P-*b*-C-*b*-F** and **P-*b*-F-*b*-C** and the protons of bis-β-CD (Figures S15 and S16). This clearly suggested the absence of orthogonal chain collapse mediated by host−guest interactions in the triblock polymers,

https://doi.org/10.1021/acspolymersau.4c00009
ACS Polym. Au 2024, 4, 255−265

as the host did not show any selectivity over coumarin or ferrocene. This was corroborated with DLS data that revealed a considerable reduction in particle size (in the range of 55−70 nm) for all of the triblock polymers, indicating the nonspecific nature of the position of coumarin or ferrocene in block copolymers in forming inclusion complexes with bis-β-CD (Figure 5D). The TEM image showed the transformation of the vesicles to micelles (diameter ∼70 nm) for **P-*b*-C-*b*-F** upon forming the inclusion complex (Figure 5E). The host−-guest-mediated chain collapse led to a decrease in the volume of hydrophobic blocks with a consequent lowering of the packing parameter value that in turn resulted in a structural transformation from vesicles to micelles.

Further, we employed the Langmuir−Blodgett experiment to monitor the variations in the pressure−area isotherms of the sequence-specific triblock polymers and their stimuli-responsive behavior to alter the nature of the isotherm. Interestingly, we observed a pseudoplateau for segmented triblock polymers **P-*b*-F-*b*-C** and **P-*b*-C-*b*-F** below the range of 140 Å^2 per repeating polymer unit, indicating the formation of similar morphological structures, i.e., vesicles, that was corroborated by morphological evidence (Figure 6A). However, random diblock polymer of **P-*b*-C-*r*-F** exhibited multiple transitions in the range of 175−140 Å^2 per repeating polymer unit. This clearly suggested the efficient packing between the compatible blocks in segmented triblock polymers in the monolayer, whereas in the case of a random diblock system, the existence of multiple plateau conditions signified irregular packing between coumarin and ferrocene blocks due to their random orientation in the hydrophobic block. Next, the monolayer of **P-*b*-F-*b*-C** was subjected to photo and redox stimuli in an orthogonal manner that exhibited a significant difference in the Langmuir isotherm pattern (Figure 6B). Thus, upon irradiation with UV_B light, polymer **P-*b*-F-*b*-C** with coumarin in the peripheral block exhibited a decrease in the maximum surface pressure from 44 to 31 mN/m, signifying a morphological transformation from vesicles to micelles in corroboration with spectroscopic and microscopic evidence. However, redox cue did not render any change in the surface pressure underscoring the importance of sequence specificity in the hydrophobic block's response to external stimuli. Similarly, **P-*b*-C-*b*-F** with ferrocene in the peripheral block exhibited much higher redox responsiveness with a reduction in surface pressure from 39 to 27 mN/m as compared to photo response (Figure 6C). For random polymer **P-*b*-C-*r*-F**, we could not observe any significant change in the Langmuir isotherm in response to the photo cue; however, a slight increase in the surface pressure was observed upon oxidation (Figure 6D). Such behavior could be attributed to the swelling of micelles due to the enhanced interaction of the ferrocenium cation, as evident from spectroscopic and morphological analyses.

CONCLUSIONS

In summary, we designed sequence-specific combinations of triblock segmented polymers **P-*b*-C-*b*-F** and **P-*b*-F-*b*-C** and diblock polymer **P-*b*-C-*r*-F** with light-responsive coumarin and redox-responsive ferrocene motifs located within hydrophobic blocks of the copolymer using RAFT chain extension polymerization. The native polymers self-assembled into vesicles by virtue of their packing parameter, as dictated by the hydrophobic−hydrophilic block composition and architecture. Interestingly, by exploiting the orthogonality of light and redox cues toward coumarin and ferrocene, we could bring selective chain action of the hydrophobic blocks, leading to alterations in the packing parameter values. This rendered structural transformation from vesicles to micelles, which was studied in detail using UV−vis spectroscopy, DLS, CV, and Langmuir isotherms to underline the importance of sequence specificity in block copolymers. Interestingly, chemical stimuli implying host−guest interactions with bis-β-CD could not distinguish between otherwise orthogonal coumarin and ferrocene, thereby leading to chain collapse with a subsequent variation of the packing parameter value in triblock polymers **P-*b*-C-*b*-F** and **P-*b*-F-*b*-C** and random diblock polymer **P-*b*-C-*r*-F**. The selective chain collapse of the chains imparted orthogonal control in the stimuli-responsive transformation of self-assembled vesicles into micelles in response to the choice of external stimuli. Thus, we have successfully demonstrated the role of sequence specificity in block copolymers toward orthogonal stimuli to furnish compartments in polymeric nanostructures that could find its eventual implication in mimicking artificial cell models interacting with extracellular matrices.

ASSOCIATED CONTENT

Supporting Information

The Supporting Information is available free of charge at https://pubs.acs.org/doi/10.1021/acspolymersau.4c00009.

Synthesis and characterization of the polymers; NMR spectra; SEC data; DLS; and UV−vis spectra to monitor polymer nanostructure formation (PDF)

AUTHOR INFORMATION

Corresponding Author

Asish Pal − *Chemical Biology Unit, Institute of Nano Science and Technology, Mohali, Punjab 140306, India;* orcid.org/0000-0002-6158-1158; Email: apal@inst.ac.in

Authors

Chirag Miglani − *Chemical Biology Unit, Institute of Nano Science and Technology, Mohali, Punjab 140306, India*

Jahanvi Ralhan − *Chemical Biology Unit, Institute of Nano Science and Technology, Mohali, Punjab 140306, India*

Maqsuma Banoo − *Department of Chemical Sciences, IISER Mohali, Mohali, Punjab 140306, India*

Debasish Nath − *Chemical Biology Unit, Institute of Nano Science and Technology, Mohali, Punjab 140306, India*

Soma Sil − *Department of Chemical Sciences, IISER Mohali, Mohali, Punjab 140306, India*

Santanu K. Pal − *Department of Chemical Sciences, IISER Mohali, Mohali, Punjab 140306, India;* orcid.org/0000-0003-4101-4970

Ujjal K. Gautam − *Department of Chemical Sciences, IISER Mohali, Mohali, Punjab 140306, India;* orcid.org/0000-0002-0731-0429

Complete contact information is available at: https://pubs.acs.org/10.1021/acspolymersau.4c00009

Author Contributions

A.P. conceived the idea of the work along with C.M., who performed most of the work with the help of the other coauthors. M.B. under the supervision of U.K.G. performed the TEM measurements. J.R. and S.S. under the supervision of S.P.

https://doi.org/10.1021/acspolymersau.4c00009
ACS Polym. Au 2024, 4, 255−265

performed the LB measurements. D.N. performed CV. The manuscript was written by C.M., J.R., and A.P. CRediT: **Chirag Miglani** conceptualization, formal analysis, investigation, writing-original draft; **Jahanvi Ralhan** conceptualization, data curation, formal analysis, investigation, writing-original draft, writing-review & editing; **Maqsuma Banoo** data curation, formal analysis, investigation; **Debasish Nath** data curation, formal analysis, methodology; **Soma Sil** data curation, formal analysis, methodology; **Santanu Kumar Pal** supervision, validation; **Ujjal K. Gautam** formal analysis, supervision, validation; **Asish Pal** conceptualization, formal analysis, funding acquisition, project administration, resources, supervision, writing-original draft, writing-review & editing.

Funding

The work was financially supported by the Department of Science & Technology DST, SERB project CRG/2020/004251 and CRG/2021/001420.

Notes

The authors declare no competing financial interest.

■ ACKNOWLEDGMENTS

The authors thank Institute of Nano Science and Technology (INST), Mohali, for providing infrastructure and characterization facilities. AP thanks the Department of Science & Technology (DST, SERB project CRG/2020/004251) for financial support. U.K.G. gratefully acknowledges support from SERB under Grant No. CRG/2021/001420. M.B. thanks CSIR (India) for the senior research fellowship. J.R. acknowledges the CSIR 09/1129(12883)/2021-EMR-I for fellowship.

■ REFERENCES

(1) Levitt, M.; Gerstein, M.; Huang, E.; Subbiah, S.; Tsai, J. Protein folding: the endgame. *Annu. Rev. Biochem.* **1997**, *66*, 549−579.
(2) Baldwin, R. L.; Rose, G. D. Is protein folding hierarchic? I. Local structure and peptide folding. *Trends Biochem. Sci.* **1999**, *24*, 26−33.
(3) Nassar, R.; Dignon, G. L.; Razban, R. M.; Dill, K. A. The protein folding problem: The role of theory. *J. Mol. Biol.* **2021**, *433*, No. 167126.
(4) Dill, K. A.; MacCallum, J. L. The protein-folding problem, 50 years on. *Science* **2012**, *338*, 1042−1046.
(5) Lutz, J.-F.; Ouchi, M.; Liu, D. R.; Sawamoto, M. Sequence-controlled polymers. *Science* **2013**, *341*, No. 1238149.
(6) Badi, N.; Lutz, J.-F. Sequence control in polymer synthesis. *Chem. Soc. Rev.* **2009**, *38*, 3383−3390.
(7) Lutz, J.-F.; Lehn, J.-M.; Meijer, E. W.; Matyjaszewski, K. From precision polymers to complex materials and systems. *Nat. Rev. Mater.* **2016**, *1*, No. 16024.
(8) Quinn, J. D.; Register, R. A. Microphase separation in block-random copolymers of styrene, 4-acetoxystyrene, and 4-hydroxystyrene. *J. Polym. Sci., Part B: Polym. Phys.* **2009**, *47*, 2106−2113.
(9) Beckingham, B. S.; Register, R. A. Synthesis and phase behavior of block-random copolymers of styrene and hydrogenated isoprene. *Macromolecules* **2011**, *44*, 4313−4319.
(10) Kim, J.; Gray, M. K.; Zhou, H.; Nguyen, S. T.; Torkelson, J. M. Polymer blend compatibilization by gradient copolymer addition during melt processing: Stabilization of dispersed phase to static coarsening. *Macromolecules* **2005**, *38*, 1037−1040.
(11) Wong, C. L. H.; Kim, J.; Torkelson, J. M. Breadth of glass transition temperature in styrene/acrylic acid block, random, and gradient copolymers: Unusual sequence distribution effects. *J. Polym. Sci., Part B: Polym. Phys.* **2007**, *45*, 2842−2849.
(12) Jouenne, S.; Gonzalez-Leon, J. A.; Ruzette, A.-V.; Lodefier, P.; Tence-Girault, S.; Leibler, L. Styrene/butadiene gradient block copolymers: molecular and mesoscopic structures. *Macromolecules* **2007**, *40*, 2432−2442.
(13) Mastroianni, S. E.; Epps, T. H., Iii Interfacial manipulations: controlling nanoscale assembly in bulk, thin film, and solution block copolymer systems. *Langmuir* **2013**, *29*, 3864−3878.
(14) Singh, N.; Tureau, M. S.; Epps, T. H., Iii Manipulating ordering transitions in interfacially modified block copolymers. *Soft Matter* **2009**, *5*, 4757−4762.
(15) Roy, R.; Park, J. K.; Young, W.-S.; Mastroianni, S. E.; Tureau, M. S.; Epps, T. H., Iii Double-gyroid network morphology in tapered diblock copolymers. *Macromolecules* **2011**, *44*, 3910−3915.
(16) Bisht, A. S.; Maity, P.; Roy, R. K. Comparison of Thermoresponsive Behavior between Polyproline and Periodically Grafted Polyproline toward Hofmeister Ions: An Explanation of Its Conformational Origin. *Macromolecules* **2023**, *56*, 3922−3930.
(17) Tsukahara, Y.; Nakamura, N.; Hashimoto, T.; Kawai, H.; Nagaya, T.; Sugimura, Y.; Tsuge, S. Structure and properties of tapered block polymers of styrene and isoprene. *Polym. J.* **1980**, *12*, 455−466.
(18) Lutz, J. F.; Schmidt, B. V. K. J.; Pfeifer, S. Tailored polymer microstructures prepared by atom transfer radical copolymerization of styrene and N-substituted maleimides. *Macromol. Rapid Commun.* **2011**, *32*, 127−135.
(19) Patterson, A. L.; Danielsen, S. P. O.; Yu, B.; Davidson, E. C.; Fredrickson, G. H.; Segalman, R. A. Sequence effects on block copolymer self-assembly through tuning chain conformation and segregation strength utilizing sequence-defined polypeptoids. *Macromolecules* **2019**, *52*, 1277−1286.
(20) Nakajima, M.; Nakajima, H.; Fujiwara, T.; Kimura, Y.; Sasaki, S. Nano-structured micelle particles of polylactide-poly (oxyethylene) block copolymers with different block sequences: Specific influence of stereocomplex formation of the polylactide blocks. *Polym. J.* **2015**, *66*, 160−166.
(21) Seo, Y.; Brown, J. R.; Hall, L. M. Effect of tapering on morphology and interfacial behavior of diblock copolymers from molecular dynamics simulations. *Macromolecules* **2015**, *48*, 4974−4982.
(22) Ganesan, V.; Kumar, N. A.; Pryamitsyn, V. Blockiness and sequence polydispersity effects on the phase behavior and interfacial properties of gradient copolymers. *Macromolecules* **2012**, *45*, 6281−6297.
(23) Chang, L.-W.; Lytle, T. K.; Radhakrishna, M.; Madinya, J. J.; Vélez, J.; Sing, C. E.; Perry, S. L. Sequence and entropy-based control of complex coacervates. *Nat. Commun.* **2017**, *8*, No. 1273.
(24) Unsal, H.; Onbulak, S.; Calik, F.; Er-Rafik, M.; Schmutz, M.; Sanyal, A.; Rzayev, J. Interplay between Molecular Packing, Drug Loading, and Core Cross-Linking in Bottlebrush Copolymer Micelles. *Macromolecules* **2017**, *50*, 1342−1352.
(25) Israelachvili, J. N. *Intermolecular and Surface Forces*; Academic Press, 1991.
(26) Moughton, A. O.; O'Reilly, R. K. Thermally Induced Micelle to Vesicle Morphology Transition for a Charged Chain End Diblock Copolymer. *Chem. Commun.* **2010**, *46*, 1091−1093.
(27) Yao, H.; Ning, Y.; Jesson, C. P.; He, J.; Deng, R.; Tian, W.; Armes, S. P. Using Host−Guest Chemistry to Tune the Kinetics of Morphological Transitions Undertaken by Block Copolymer Vesicles. *ACS Macro Lett.* **2017**, *6*, 1379−1385.
(28) Liu, Y.; Pujals, S.; Stals, P. J. M.; Paulöhrl, T.; Presolski, S. I.; Meijer, E. W.; Albertazzi, L.; Palmans, A. R. A. Catalytically Active Single-Chain Polymeric Nanoparticles: Exploring Their Functions in Complex Biological Media. *J. Am. Chem. Soc.* **2018**, *140*, 3423−3433.
(29) Romulus, J.; Weck, M. Single-Chain Polymer Self-Assembly Using Complementary Hydrogen Bonding Units. *Macromol. Rapid Commun.* **2013**, *34*, 1518−1523.
(30) Deane, O. J.; Jennings, J.; Neal, T. J.; Musa, O. M.; Fernyhough, A.; Armes, S. P. Synthesis and Aqueous Solution Properties of Shape-Shifting Stimulus-Responsive Diblock Copolymer Nano-Objects. *Chem. Mater.* **2021**, *33*, 7767−7779.
(31) Zhang, J.; Farias-Mancilla, B.; Kulai, I.; Hoeppener, S.; Lonetti, B.; Prevost, S.; Ulbrich, J.; Destarac, M.; Colombani, O.; Schubert, U. S.; Guerrero-Sanchez, C.; Harrison, S. Effect of Hydrophilic

Monomer Distribution on Self-Assembly of a pH-Responsive Copolymer: Spheres, Worms and Vesicles from a Single Copolymer Composition. *Angew. Chem., Int. Ed.* **2021**, *60*, 4925−4930.
(32) Zhang, Y.; Tang, Y.; Zhang, J.; Harrisson, S. Amphiphilic Asymmetric Diblock Copolymer with pH-Responsive Fluorescent Properties. *ACS Macro Lett.* **2021**, *10*, 1346−1352.
(33) Joseph, J. P.; Miglani, C.; Singh, A.; Gupta, D.; Pal, A. Photoresponsive chain collapse in a flexo−rigid functional copolymer to modulate the self-healing behaviour. *Soft Matter* **2020**, *16*, 2506−2515.
(34) Miglani, C.; Joseph, J. P.; Gupta, D.; Singh, A.; Pal, A. Modulation of flexo-rigid balance in photoresponsive thymine grafted copolymers towards designing smart healable coating. *RSC Adv.* **2021**, *11*, 39376−39386.
(35) Joseph, J. P.; Miglani, C.; Bhatt, A.; Ray, D.; Singh, A.; Gupta, D.; Ali, M. E.; Aswal, V. K.; Pal, A. Delineating Synchronized Control of Dynamic Covalent and Non-Covalent Interactions for Polymer Chain Collapse Towards Cargo Localization and Delivery. *Polym. Chem.* **2021**, *12*, 1002−1013.
(36) Nath, D.; Ralhan, J.; Joseph, J. P.; Miglani, C.; Pal, A. Thermoresponsive Injectable Hydrogel To Mimic the Heat-and Strain-Stiffening Behavior of Biopolymers toward Muscle Cell Proliferation. *Biomacromolecules* **2024**, *25*, 853−863.
(37) Joseph, J. P.; Gupta, N.; Miglani, C.; Nath, D.; Singh, A.; Gupta, D.; Pal, A. Unraveling On-demand Strain-Stiffening in Nanofibrous Peptide−Polymer Conjugates to Mimic Contractility in Actinomyosin Networks. *Chem. Mater.* **2022**, *34*, 4364−4374.
(38) Gupta, D.; Gupta, V.; Nath, D.; Miglani, C.; Mandal, D.; Pal, A. Stimuli-responsive self-assembly disassembly in peptide amphiphiles to endow block-co-fibers and tunable piezoelectric response. *ACS Appl. Mater. Interfaces* **2023**, *15*, 25110−25121.
(39) Gupta, D.; Bhatt, A.; Gupta, V.; Miglani, C.; Joseph, J. P.; Ralhan, J.; Mandal, D.; Ali, M. E.; Pal, A. Photochemically Sequestered Off-Pathway Dormant States of Peptide Amphiphiles for Predictive On-Demand Piezoresponsive Nanostructures. *Chem. Mater.* **2022**, *34*, 4456−4470.
(40) Miglani, C.; Banoo, M.; Nath, D.; Ralhan, J.; Sil, S.; Joseph, J. P.; Pal, S. K.; Gautam, U.; Pal, A. Orthogonal Chain Collapse in Stimuli-Responsive Di-Block Polymers Leading to Self-Sorted Nanostructures. *Chem. Commun.* **2023**, *59*, 13195−13198.
(41) Maulik, A.; Miglani, C.; Mavlankar, N. A.; Joseph, J. P.; Chandran, V. C.; Pal, A. Topochemical polymerization in phenylalanine anchored chiral diacetylenes for chiroptical properties and tunable thermo-, halo-, solvatochromism. *New J. Chem.* **2023**, *47*, 1657−1665.
(42) Joseph, J. P.; Miglani, C.; Maulik, A.; Abraham, S. R.; Dutta, A.; Baev, A.; Prasad, P. N.; Pal, A. Stereoselective Plasmonic Interaction in Peptide-tethered Photopolymerizable Diacetylenes Doped with Chiral Gold Nanoparticles. *Angew. Chem., Int. Ed.* **2023**, *62*, No. e202306751.
(43) Gupta, D.; Sasmal, R.; Singh, A.; Joseph, J. P.; Miglani, C.; Agasti, S. S.; Pal, A. Enzyme-responsive chiral self-sorting in amyloid-inspired minimalistic peptide amphiphiles. *Nanoscale* **2020**, *12*, 18692−18700.
(44) Paul, A.; Borrelli, R.; Bouyanfif, H.; Gottis, S.; Sauvage, F. Tunable redox potential, optical properties, and enhanced stability of modified ferrocene-based complexes. *ACS Omega* **2019**, *4*, 14780−14789.
(45) Pietschnig, R. Polymers with pendant ferrocenes. *Chem. Soc. Rev.* **2016**, *45*, 5216−5231.
(46) Blanazs, A.; Armes, S. P.; Ryan, A. J. Self-Assembled Block Copolymer Aggregates: From Micelles to Vesicles and Their Biological Applications. *Macromol. Rapid Commun.* **2009**, *30*, 267−277.
(47) Kim, B. Y.; Ratcliff, E. L.; Armstrong, N. R.; Kowalewski, T.; Pyun, J. Ferrocene Functional Polymer Brushes on Indium Tin Oxide via Surface-Initiated Atom Transfer Radical Polymerization. *Langmuir* **2010**, *26*, 2083−2092.
(48) Alkan, A.; Wald, S.; Louage, B.; De Geest, B. G.; Landfester, K.; Wurm, F. R. Amphiphilic Ferrocene-Containing PEG Block Copolymers as Micellar Nanocarriers and Smart Surfactants. *Langmuir* **2017**, *33*, 272−279.
(49) Liu, L.; Rui, L.; Gao, Y.; Zhang, W. Self-Assembly and Disassembly of a Redox-Responsive Ferrocene-Containing Amphiphilic Block Copolymer for Controlled Release. *Polym. Chem.* **2015**, *6*, 1817−1829.
(50) Saleem, M.; Wang, L.; Yu, H.; Akram, M.; Ullah, R. S. Synthesis of amphiphilic block copolymers containing ferrocene−boronic acid and their micellization, redox-responsive properties and glucose sensing. *Colloid Polym. Sci.* **2017**, *295*, 995−1006.

https://doi.org/10.1021/acspolymersau.4c00009
ACS Polym. Au 2024, 4, 255−265